nature synthesis

Article

https://doi.org/10.1038/s44160-023-00384-6

Mechanism-guided realization of selective carbon monoxide electroreduction to methanol

Received: 17 March 2023

Accepted: 25 July 2023

Published online: 28 August 2023

Check for updates

Jing Li[1,2], Bo Shang[1,2], Yuanzuo Gao[1,2], Seonjeong Cheon[1,2], Conor L. Rooney[1,2] & Hailiang Wang[1,2]

Cobalt phthalocyanine can effectively convert CO_2 or CO to methanol. However, this reaction is hampered by low selectivity (a methanol Faradaic efficiency of less than 40%) and poor understanding of the kinetics and mechanism. In this work, we use a mechanism-guided reaction design approach based on systematic kinetic studies to overcome these limitations. pH-dependent Tafel analysis and kinetic isotopic effect experiments explain that methanol production from CO electroreduction is pH independent and limited by the *CO hydrogenation to *CHO step with H_2O as the major proton source. Proton donor comparisons show that bicarbonate can promote the reaction at its optimal concentration of 0.1 M and CO reaction order studies confirm a Henry type isotherm for CO adsorption on the catalyst surface. These mechanistic findings lead us to carry out CO reduction in a 0.1 M bicarbonate electrolyte, under 10 atm CO pressure and with a microporous layer on the electrode to enhance reactant transport. Our reaction achieves a high methanol Faradaic efficiency of 84% with a partial current density of more than 20 mA cm^{-2} at −0.98 V versus the reversible hydrogen electrode, making the electrochemical CO-to-methanol conversion a selective process viable for practical application.

Electrochemical reduction of CO_2 to commodity chemicals and fuels provides a promising technical solution to generate valuable products from an abundant pollutant and to realize a sustainable economy[1–6]. Substantial progress has been made on heterogeneous metallic catalysts (including Cu, Ag, Au, Bi) for converting CO_2 into a variety of value-added products such as carbon monoxide (CO), formic acid/formate ($HCOOH/HCOO^-$), methane (CH_4), ethanol (CH_3CH_2OH) and ethylene (C_2H_4)[7–13]. However, the presence of many different sites on metal surfaces is a challenge to mechanistic studies. Molecular catalysts are a promising alternative because their well-defined structures provide a precise model for theoretical calculations and experimental studies to understand the reaction mechanism and thereby improve the catalytic performance[14–18]. Many molecular catalysts with various transition metal centres such as Co, Ni, Fe and Mn have been reported to show appreciable activity in CO_2 electroreduction[19–24]. Most of them generate two-electron reduction products such as CO and formate. Further reduced products, although desirable, are hard to obtain.

Our previous work developed a molecular electrocatalyst[25], consisting of amine-substituted cobalt phthalocyanine molecules supported on carbon nanotubes (CoPc-NH_2/CNT), that can stably reduce CO_2 to methanol (CH_3OH) in substantial yield. The catalytic activity was proposed to be intrinsic to the CoPc-NH_2 molecule and greatly enhanced by its electronic coupling with the highly conductive CNT support[15]. Following this initial work, many more efforts have been devoted to understanding and developing the reaction of CO_2 or CO reduction to methanol catalysed by CoPc-based materials[26–32].

[1]Department of Chemistry, Yale University, New Haven, CT, USA. [2]Energy Sciences Institute, Yale University, West Haven, CT, USA.
e-mail: hailiang.wang@yale.edu

https://doi.org/10.1038/s44160-023-00384-6

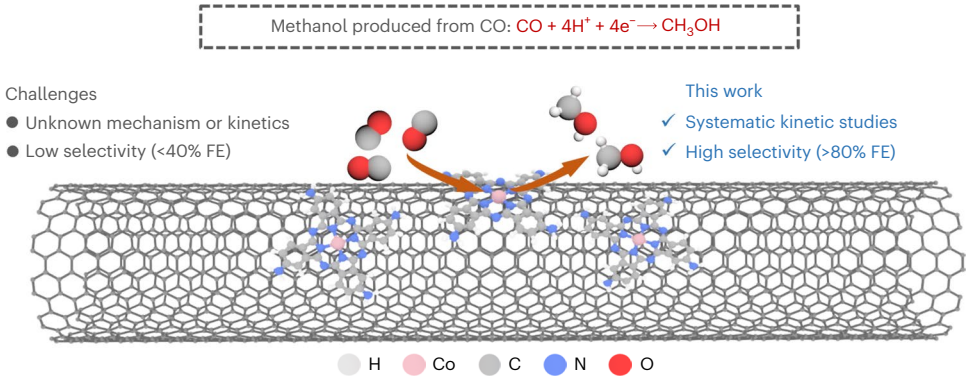

Fig. 1 | CO-to-CH_3OH conversion catalysed by CoPc-NH_2/CNT, and the current challenges and progress made in this work. The catalyst consists of CoPc-NH_2 molecules highly dispersed on CNT surfaces. This work increased methanol FE from less than 40% to more than 80% using strategies formulated from electrochemical kinetic studies.

However, the reaction kinetics and mechanism are not understood except that CO and formaldehyde are reaction intermediates and that CO reduction is probably rate-limiting, which hampers further improvement of the catalytic performance (Fig. 1). Thus far, the highest methanol selectivity (Faradaic efficiency, FE) achieved in CO_2/CO reduction has been approximately 40% (ref. 25) due to the sluggish CO reduction and competition from the hydrogen evolution reaction (HER), which is well below the standard of practical application.

In this work, we performed systematic kinetic studies of CO electroreduction catalysed by CoPc-NH_2/CNT and successfully leveraged the derived mechanistic understanding to considerably improve the FE of methanol production to more than 80%. In response to the reactant's low solubility in aqueous electrolyte, we first introduced a microporous layer (MPL) into the catalytic electrode structure, which enhanced the mass transport of CO and increased the methanol FE from 40 to 66%. Tafel analysis revealed an unvarying slope close to 118 mV dec^{-1} for methanol production at electrolyte pH from 7 to 13, indicating that transfer of the first electron to CO is the rate-determining step (RDS). pH dependence and isotopic labelling experiments suggested that H_2O is involved as the major proton source in the RDS, although the presence of bicarbonate (HCO_3^-) can further enhance proton transfer. A pressure dependence study showed that the methanol generation reaction is first order with respect to CO partial pressure, indicating a Henry type isotherm for CO adsorption on the catalyst surface. These mechanistic findings inspired us to carry out CO reduction under high-pressure conditions in $KHCO_3$ electrolyte and achieved a high methanol FE of 84% with a partial current density of more than 20 mA cm^{-2} at −0.98 V versus the reversible hydrogen electrode (RHE; all potentials in this paper are referred to RHE unless otherwise stated).

Results and discussion

Electrocatalytic properties of CoPc-NH_2/CNT for CO reduction

Our previous work has shown that CO is always present in the products of CO_2 reduction to methanol, and that CO reduction to methanol requires a larger overpotential than CO_2 reduction to CO (refs. 19,25). This suggests that CO reduction to methanol is a more sluggish reaction than CO_2 reduction to CO, which agrees with the observation that most metal-N_4 molecular electrocatalysts can only convert CO_2 to CO (refs. 20,21,23,33). Therefore, in this work we isolate the CO electroreduction reaction for investigation. We note that CO does not react with any commonly used electrolyte, and thus can facilitate reliable electrokinetic measurements in a wide pH range. Considering that the reactant is poorly soluble in aqueous electrolyte, we first sought to enhance the mass transport of CO by introducing a MPL consisted of carbon particles and fluoropolymers into the electrode structure (Fig. 2a). Not only does the inclusion of the MPL increase the diffusion limited current for CO reduction to enable reliable kinetic measurements, it may also steer some CoPc-NH_2 sites from catalysing HER to catalysing CO reduction.

Measured at ambient temperature and pressure (pressure is 1 atm in all experiments unless specifically stated otherwise) in a 0.1 M CO-saturated $KHCO_3$ aqueous solution, the CoPc-NH_2/CNT catalyst manifests clear potential dependence in the range of −0.62 to −0.93 V (Fig. 2b). Methanol and H_2 are the only two products detected, which indicates a single reaction pathway from CO to methanol, a notable characteristic of molecular catalysts. As the applied potential decreases from −0.62 to −0.80 V, the methanol FE increases substantially from 12 to 66% whereas the H_2 FE decreases from 86 to 37%. As the potential becomes even more negative, the methanol FE gradually decreases as a result of the more competitive HER. The partial current density of methanol reaches a plateau at −0.87 and −0.90 V and then slightly decreases at −0.93 V, probably due to CO mass transport limitations. This result shows more than 50% improvement of methanol selectivity over the highest reported value, which was obtained using the same catalyst supported on carbon fibre paper without MPL coating[25]. In the potential range from −0.62 to −0.87 V, both methanol and H_2 partial current densities increase nearly exponentially from several mA cm^{-2} to more than 10 mA cm^{-2} (Fig. 2c), indicating no apparent CO mass transport limitation. This important improvement in reaction rate and selectivity, enabled by the improved microenvironment and interfaces near the catalyst, laid the foundation for further mechanistic and kinetic investigations of CO reduction to methanol catalysed by CoPc-NH_2/CNT.

Tafel analysis and kinetic isotopic effect

To probe the kinetics of methanol production, the reaction was systematically evaluated in the electrolyte pH range of 7.0 to 13.2 at electrode potentials between −0.44 and −1.0 V versus RHE: that is, between −1.14 and −1.5 V versus the standard hydrogen electrode (SHE) (Fig. 2 and Supplementary Fig. 1). The CoPc-NH_2/CNT catalyst experiences no notable deactivation during electrolysis as evidenced by the stable current profile (Supplementary Fig. 2). Total cation concentration was kept at 0.1 M in all electrolytes to cancel out any cation effect[34,35] in comparing CO reduction activity. All kinetic analysis was done in the potential range where the methanol production rate is lower than 10 mA cm^{-2} to avoid mass transport influences. According to computational and experimental work in the literature[26,27,36–39], possible RDSs of CO reduction to methanol can be summarized as follows (Table 1).

Tafel slopes for methanol production from CO reduction were determined to be all around 118 mV dec^{-1} in a wide range pH of 7.0–13.2 (Fig. 3a,b), which suggests that the reaction kinetics is limited by the initial one-electron transfer process assuming a symmetry factor of 0.5. Thus, the rate-limiting chemical step (A2) involving the recombination

https://doi.org/10.1038/s44160-023-00384-6

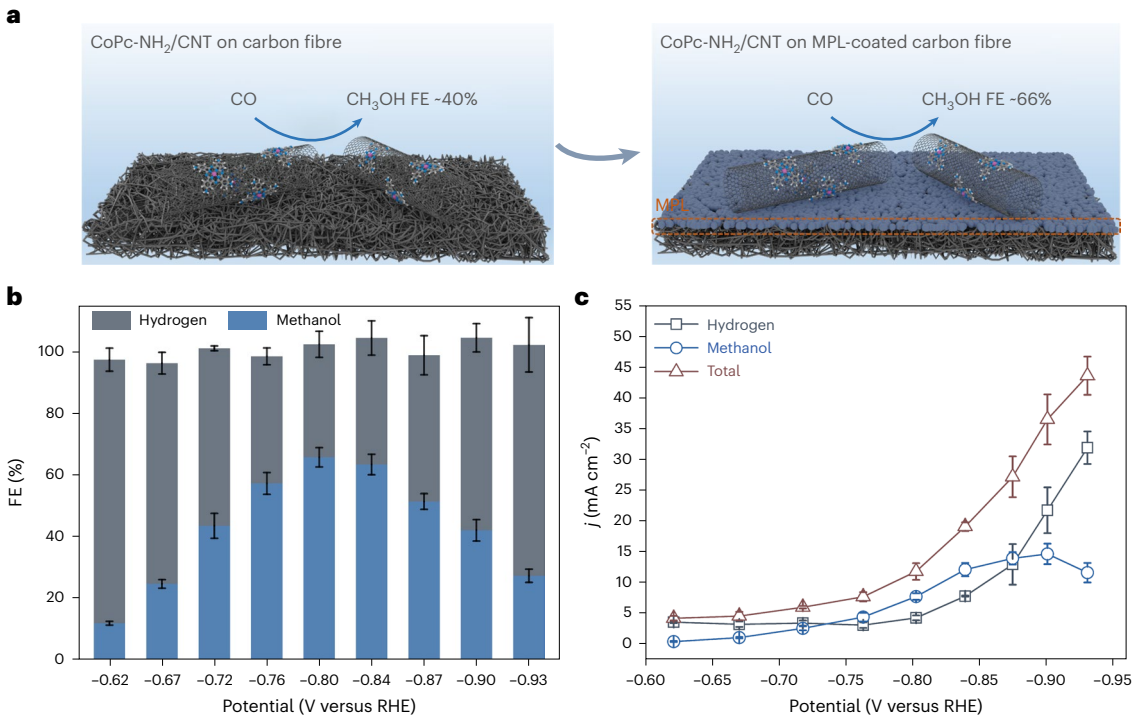

Fig. 2 | Improving methanol selectivity by enhancing CO mass transport. **a**, Schematic of CO reduction to methanol catalysed by CoPc-NH_2/CNT loaded on carbon fibre paper without (left) and with MPL coating (right). **b**,**c**, Product selectivity (FE) (**b**) and partial current density (**c**) for methanol and hydrogen versus applied electrode potential measured in 0.1 M aqueous $KHCO_3$. Data are presented as mean values and error bars represent standard deviations ($n = 3$ replicates).

Table 1 | Summary of possible RDSs for methanol formation, and their corresponding Tafel slopes

	Possible RDS	Tafel slope	pH dependent
A1	$*CO + e^- \rightarrow *CO^-$	118 mV dec^{-1}	No
A2	$*CO + *H \rightarrow *CO(H) + *$[a]	59 mV dec^{-1}	Yes
A3	$*CO + e^- + H^+ \rightarrow *CO(H)$	118 mV dec^{-1}	Yes
A4	$*CO + e^- + H_2O \rightarrow *CO(H) + OH^-$	118 mV dec^{-1}	No

[a]The asterisk represents surface sites. $*CO(H)$ denotes that the H atom can be bonded to either O or C.

between *CO and *H could be ruled out. On the RHE scale, the reaction rate of methanol formation increases with electrolyte pH at the same potential, and the Tafel curves exhibit clear pH-dependent shifts in potential (Fig. 3a). For example, the potential versus pH slope is fitted to be roughly 45–48 mV per pH unit at methanol partial current densities of 1 and 5 mA cm^{-2} (Supplementary Fig. 3). The slight difference from the ideal pH dependency of 59 mV per pH unit could be due to experimental errors and/or the proton-donating capability of some of the anions, which will be discussed later in this article. Consistently, the Tafel curves show much smaller potential shifts in response to pH variation on the SHE scale (Fig. 3b). The observation that the measured Tafel curves manifest a substantial pH dependence on the RHE scale but a much smaller pH dependence on the SHE scale suggests that the production rate of methanol is mostly pH independent. These results lead to the conclusion that the RDS and its previous steps of the major reaction pathway should not involve H^+. Thus, the electron transfer step (A1) and the proton-coupled electron transfer (PCET) step (A4) in which H_2O is the proton source are viable RDS candidates.

To further confirm the RDS of methanol formation, the reaction rates in $KHCO_3/H_2O$ and $KDCO_3/D_2O$ electrolytes were compared. As shown in Fig. 3c, the formation rate of methanol at the same applied potential is severely suppressed when changing from $KHCO_3/H_2O$ to $KDCO_3/D_2O$. Since the O–H bond has a higher zero-point energy than the O–D bond, this kinetic H/D isotope effect indicates that the reaction rate is limited by proton transfer, probably from water. We further performed CO reduction in 0.1 M $KHCO_3$ electrolytes with H_2O-acetonitrile and H_2O-acetone mixed solvents. As shown in Supplementary Fig. 4, the partial current density of methanol decreases with the concentration of H_2O, which verifies that the reduction of CO to methanol is affected by the activity of H_2O as the major proton source. Thus, we can rule out A1, which has no proton transfer involved. Therefore, the PCET step (A4) is the most viable RDS that satisfies all the experimental observations. The proton transfer can occur at the C or O atom of the adsorbed CO to form *CHO or *COH, respectively (Fig. 3d). Our recent discovery of the direct electrosynthesis of methylamine from carbon dioxide and nitrate catalysed by CoPc-NH_2/CNT corroborates that methanol is formed from CO_2 reduction through a formaldehyde pathway[40]. Therefore, *CHO is the more likely product of the RDS in this case.

Proton donor effect on methanol production

Since the RDS of CO reduction to methanol was found to involve proton transfer, we further investigated the effect of different proton donors. First, we compared the partial current density of methanol in different electrolytes at the same moderate potential of −1.35 V versus SHE (Fig. 4a). The K_2HPO_4/KH_2PO_4 and $KHCO_3$ electrolytes give notably higher methanol current than the K_2CO_3 and KOH electrolytes, reflecting the effect of proton donors. Note that H_2O is the sole proton donor in the last two electrolytes, and therefore they show comparable methanol rates. Further comparison reveals that $KHCO_3$ exhibits higher activity and selectivity towards methanol formation than K_2HPO_4/KH_2PO_4, indicating that HCO_3^- is a better proton source than $H_2PO_4^-/HPO_4^{2-}$ for the electroreduction of CO to methanol.

https://doi.org/10.1038/s44160-023-00384-6

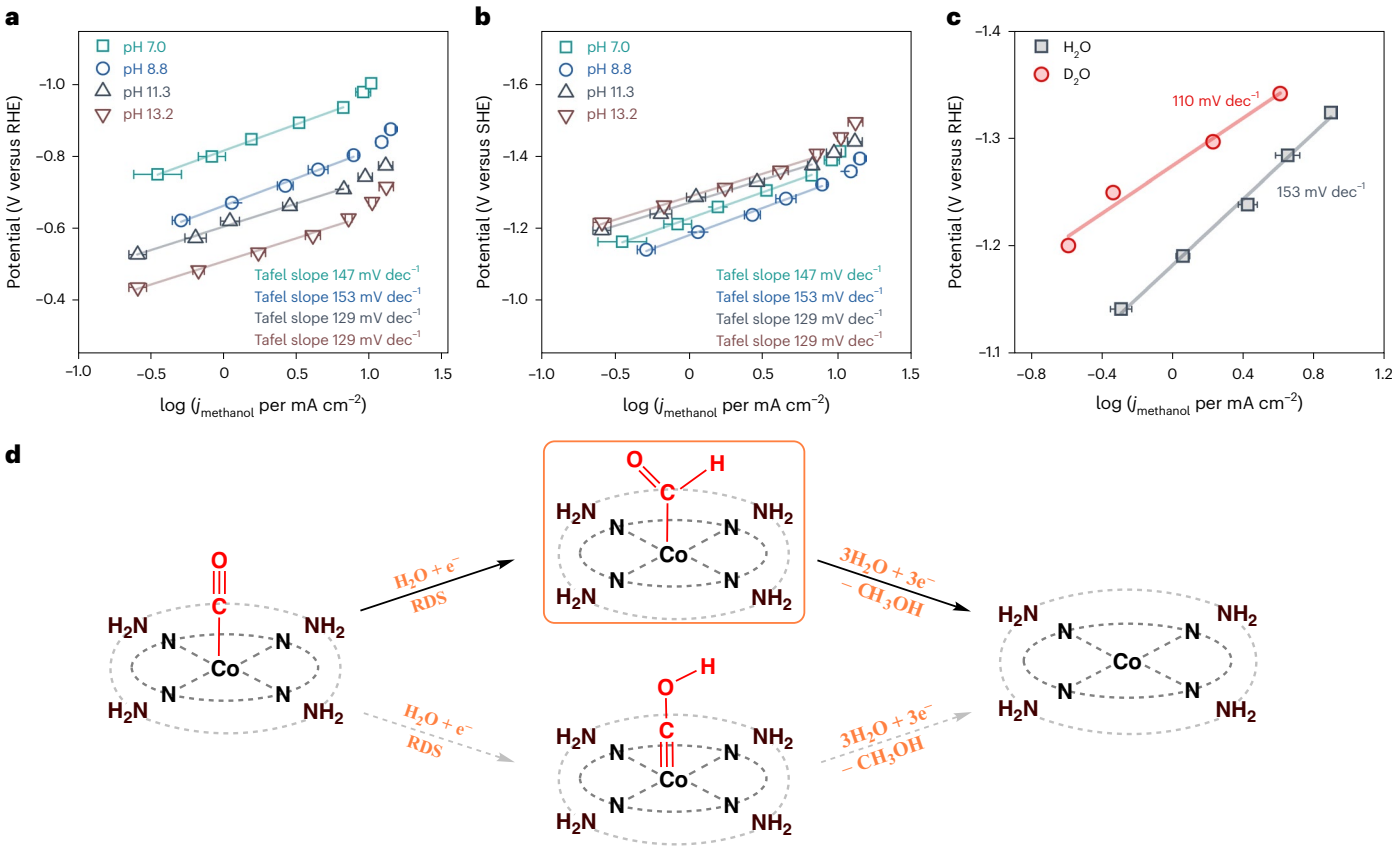

Fig. 3 | Kinetic analysis for methanol production from CO electroreduction catalysed by CoPc-NH_2/CNT. a,**b**, The RHE scale (**a**) and the SHE scale (**b**) Tafel curves for methanol formation at different electrolyte pH. **c**, Isotopic labelling experiments measured in $KHCO_3/H_2O$ and $KDCO_3/D_2O$ electrolytes. **d**, Schematic of reaction pathways leading to methanol based on the kinetic results. Data are presented as mean values and error bars represent standard deviations ($n = 3$ replicates).

Then we determined the reaction orders of methanol and H_2 formation with respect to the concentrations of HCO_3^- and $H_2PO_4^-$ in the range of 0.01 to 0.1 M, with $KClO_4$ added to the electrolyte when needed to maintain a constant cation strength of 0.1 M. Methanol production shows a 0.33 order dependence on [HCO_3^-] throughout the entire concentration range (Fig. 4b), whereas a lower order of 0.22 from 0.01 to 0.04 M and a near zero order at concentrations higher than 0.04 M are found with respect to $H_2PO_4^-$ (Fig. 4b). This change in reaction order could be attributed to decreased *CO coverage caused by promoted HER competing with CO reduction for active sites and/or specific adsorption of $H_2PO_4^-$ on the catalytic site[41]. We also compared CO reduction performance in HCO_3^- versus $H_2PO_4^-$ electrolytes of the same pH. The electrolysis results show that the $H_2PO_4^-$-based electrolyte gives a much lower methanol formation rate but a comparable HER rate than the HCO_3^--based electrolyte (Supplementary Fig. 5). These results again show that HCO_3^- is a more effective proton donor in the reaction of CO reduction to methanol compared with H_2O and $H_2PO_4^-$. The less optimal performance of $H_2PO_4^-$ is attributed to its capability of enhancing the HER, which displays a 0.43 order dependence (Fig. 4c). Specific adsorption of $H_2PO_4^-$ on the catalyst surface, which decreases *CO coverage, could be another reason[41]. While both HCO_3^- and $H_2PO_4^-$ can positively influence the methanol production rate, it is important to note that the highest reaction order of methanol formation with respect to these anions is only approximately 0.3. Therefore, the major proton source in this reaction is still H_2O. As [HCO_3^-] increases to higher than 0.2 M, H_2 evolution is greatly promoted and methanol production is consequently suppressed (Supplementary Fig. 6). Therefore, 0.1 M $KHCO_3$ is the optimal electrolyte for this reaction (Fig. 4d).

Mechanism-guided realization of high methanol selectivity

To determine the reaction order with respect to CO, electrolysis experiments were conducted at a constant applied potential of −1.35 V versus SHE where no apparent CO mass transport limitation occurs, and the rate of methanol production is relatively high (Fig. 2b,c). Under the total pressure of 1 atm, the CO partial pressure (p_{CO}) was varied from 0.01 to 1 atm with N_2 as the balance gas (Fig. 5a and Supplementary Fig. 7). A plot of $\log(j_{CO})$ versus $\log(p_{CO})$ exhibits a slope of 1.06 in 0.1 M $KHCO_3$ electrolyte, indicating a first-order dependence on p_{CO}. Similar results are observed in other electrolytes with different pH values (Supplementary Fig. 8). This kind of p_{CO} dependence suggests a Henry type isotherm of CO adsorption on CoPc-NH_2/CNT, which is expected because the CoPc-NH_2 molecules are highly dispersed on CNT surfaces[25] and thus the site exclusion requirement in the Langmuirian isotherm has not occurred to limit the adsorption yet. The Henry type isotherm also indicates that the absolute CO coverage on the catalyst surface remains low at 1 atm CO and that increasing p_{CO} may be a promising way to further enhance methanol production (Fig. 5b).

Inspired by the mechanistic information obtained from the aforementioned kinetic studies, we performed CO electrolysis under high-pressure conditions in 0.1 M aqueous $KHCO_3$ using a two-compartment electrochemical cell capable of operations with gas pressure up to 60 atm (Fig. 5c). The high pressure considerably improved the selectivity of methanol from CO electroreduction. Figure 5d shows the CO electrolysis results at 10 atm CO in the potential range from −0.78 to −1.03 V. At the optimal potential of −0.98 V, methanol is produced with a high FE of 84% and a partial current density of 23.5 mA cm^{-2}. This is a twofold increase in methanol selectivity from

https://doi.org/10.1038/s44160-023-00384-6

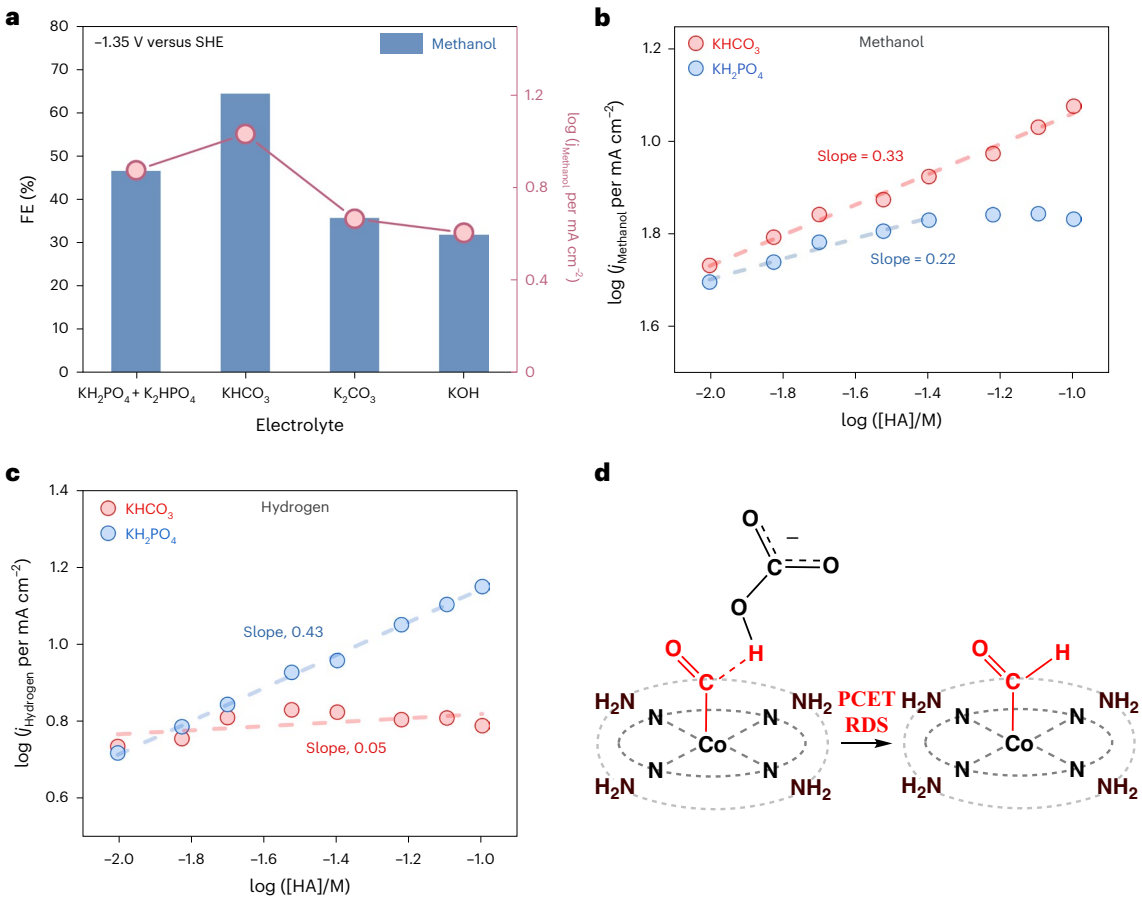

Fig. 4 | Proton donor effect on methanol production from CO electroreduction catalysed by CoPc-NH_2/CNT. a, FE and partial current density of methanol in different electrolytes. **b**,**c**, Methanol (**b**) and H_2 (**c**) partial current density versus proton donor concentration. [HA] represents either [HCO_3^-] or [$H_2PO_4^-$]. The potential for all electrolysis was kept at −1.35 V versus the SHE. **d**, Schematic of HCO_3^- as a proton donor enhancing the PCET RDS for methanol production.

the previous highest reported value. Moreover, this resolves one of the most critical issues for methanol production from electrochemical CO_2/CO reduction and brings the reaction closer to some other electrochemical reactions such as CO_2/CO reduction to CO, formate, ethylene and acetate that hold more promise for practical application in emission-to-fuel and/or chemical conversion[7,9,42–46].

Conclusions

In summary, we enhanced performance and mechanistic understanding of the CoPc-NH_2/CNT-catalysed electroreduction of CO to methanol. Initially, we increased methanol FE from roughly 40 to 60% by enhancing CO mass transport with the introduction of an MPL into the catalytic electrode structure. We then obtained understanding of the reaction mechanism through systematic kinetic experiments including pH dependence, kinetic isotopic effect, proton donor effect and CO pressure dependence. We found that methanol production from CO electroreduction is pH independent and limited by the *CO to *CHO reduction step with H_2O as the major proton source; CO adsorption on the catalyst surface follows a Henry type isotherm. The derived mechanistic information enabled us to further improve the FE of methanol production to roughly 85%.

Methods

Materials

Potassium bicarbonate ($KHCO_3$; 99%) and *N*,*N*-dimethylformamide (DMF; 99.8%) were purchased from Alfa Aesar. Potassium phosphate monobasic (KH_2PO_4; 99%), potassium phosphate dibasic (K_2HPO_4; 98%) and potassium carbonate (K_2CO_3; 98%) were purchased from Acros Organics. Potassium perchlorate ($KClO_4$; 99%) and sodium perchlorate ($NaClO_4$; 97%) were purchased from Thermo Fisher Scientific. Potassium hydroxide (KOH; 99.99% trace metals basis), sodium bicarbonate ($NaHCO_3$; 99.7%), Chelex 100 sodium form and Nafion solution (5 wt.%) were purchased from Sigma-Aldrich. Carbon monoxide (99.3%), argon (99.999%) and nitrogen (99.999%) were purchased from Airgas. Multi-walled CNTs were purchased from C-Nano (product number FT9100). The carbon paper support (Freudenberg, catalogue no. H23C6) with MPL coating was purchased from the Fuel Cell Store. The electrolyte solutions were prepared using Milli-Q water (18.2 MΩ cm^{-1} at 25 °C).

Preparation of electrolyte

The potassium cation concentrations of all electrolytes for the pH dependence study were kept at 0.1 M. The electrolytes with the pH values of 7.0, 8.8, 11.3 and 13.2 were prepared by dissolving 0.035 M K_2HPO_4 + 0.03 M KH_2PO_4, 0.1 M $KHCO_3$, 0.05 M K_2CO_3 and 0.1 M KOH in water, respectively. The electrolyte pH was determined using an Oakton pH meter (Eutech Instruments). The Chelex 100 resin was used to purify all electrolytes before electrochemical measurements.

Preparation of CoPc-NH_2/CNT hybrid catalyst

The synthesis of CoPc-NH_2 and the purification of as-purchased CNTs were carried out as detailed in our previous work[25]. To prepare the CoPc-NH_2/CNT hybrid catalyst, 30.0 mg of purified CNTs and 3 mg of CoPc-NH_2 were each dispersed in 30 ml of DMF via sonication to obtain a well-dispersed CNT suspension and a CoPc-NH_2 solution. Then, these

https://doi.org/10.1038/s44160-023-00384-6

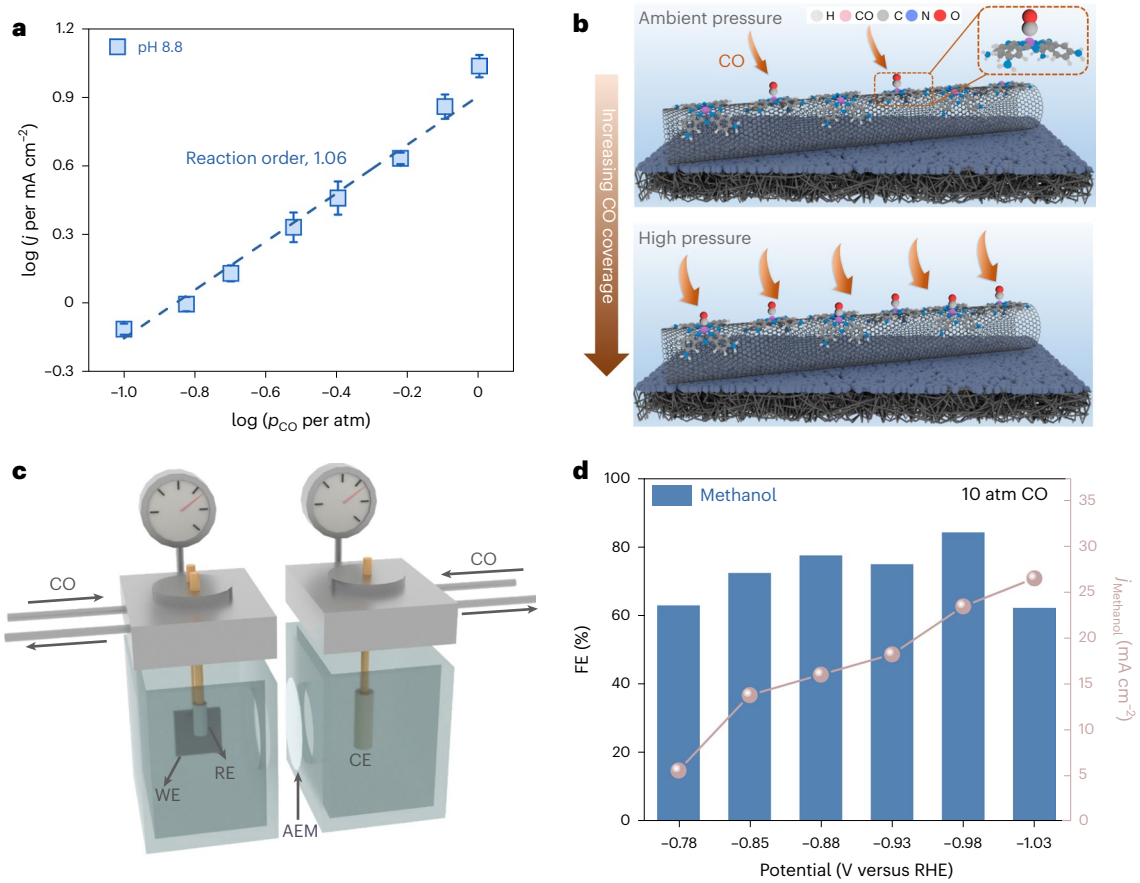

Fig. 5 | Mechanism-guided realization of high methanol selectivity. a, p_{CO} dependent methanol production rate from CO reduction catalysed by CoPc-NH_2/CNT in 0.1 M aqueous $KHCO_3$. **b**, Schematic showing that CO coverage on catalyse surface increases with CO pressure. **c**, Schematic of two-compartment high-pressure electrochemical cell used in this work. WE, RE and CE stand for working, reference and counter electrodes, respectively. AEM stands for anion exchange membrane. **d**, FE and partial current densities for methanol versus electrode potential measured under 10 atm CO in 0.1 M aqueous $KHCO_3$. Data are presented as mean values and error bars represent standard deviations ($n = 3$ replicates).

two dispersions were mixed, sonicated for 30 min and stirred for 20 h. Next, the mixture was centrifuged and the precipitate was washed using DMF and ethanol until the supernatant was transparent. Finally, the precipitate was freeze-dried to obtain the final product. The actual wight percentage of Co in the hybrid catalyst was determined to be roughly 0.67 wt.% by inductively coupled plasma mass spectrometry measurements, corresponding to roughly 10 wt.% of CoPc-NH_2.

Preparation of CoPc-NH_2/CNT electrode

An ink was first prepared by mixing 5 mg of CoPc-NH_2/CNT, 15 µl of the Nafion solution and 5 ml of ethanol followed by sonicating for 30 min. The ink solution was then drop-cast onto the carbon paper support to reach a catalyst loading of 0.4 mg cm^{-2}. Next, the as-prepared electrode was dried using an infrared lamp and cut into individual electrodes with the dimensions of roughly 0.5 × 3.0 cm^2 (catalyst covering an area of roughly 0.5 × 1.0 cm^2).

Electrocatalytic measurement

Ambient pressure electrolysis was performed in a custom-designed H-type electrochemical cell. A piece of anion-conducting membrane (Selemion DSV, AGC, Inc.) was used to separate the cathode and anode chambers. A graphite rod (Sigma-Aldrich, 99.999%) was used as the counter electrode and a Ag/AgCl (4.0 M KCl, Pine Research Instrumentation, Inc.) was used as the reference electrode. CO gas was delivered into the cathode chamber at a flow rate of 20.0 cm^3 min^{-1} using a mass flow controller (Alicat Scientific, Inc.).

High-pressure electrolysis was performed in a two-compartment electrochemical cell (Gaoss Union, Inc., P003-2). Each compartment comprised an inner Teflon chamber and a titanium shell. A platinum foil with the dimensions of 1.5 × 3.5 × 0.02 cm^3 (Gaoss Union, Inc.) was used as the counter electrode and a Ag/AgCl (saturated KCl, Gaoss Union, Inc.) was used as the reference electrode. Before electrolysis, the headspace of each compartment was purged for 5 min by delivering CO gas at a flow rate of approximately 50.0 cm^3 min^{-1}. Then, CO gas was delivered into both compartments simultaneously to reach 10 atm.

Chronopotentiometry experiments were conducted to evaluate the CO electroreduction performance using a Bio-Logic VMP3 Multichannel Potentiostat. The resistance between the working electrode and the reference electrode was determined by potentiostatic electrochemical impedance spectroscopy and then compensated automatically during measurements. Potential versus the reference electrode was converted to the RHE scale using E(versus RHE) = E(versus Ag/AgCl) + 0.199 V + 0.0591 V × pH.

Product quantification

Gas-phase products were quantified using a gas chromatograph (SRI 8610C) equipped with a flame ionization detector and a thermal conductivity detector. H_2 was quantified using thermal conductivity detector, while CO was quantified using flame ionization detector. High-purity Ar was used as the carrier gas. Gas-phase products were accumulated in a Tedlar gas sampling bag (SKC Inc.) and sampled using a gastight syringe (Hamilton) for gas chromatography analysis.

Liquid products were quantified by a Bruker AVIII 400 MHz nuclear magnetic resonance (NMR) spectrometer with water suppression. NMR samples were prepared by mixing 450 µl of the electrolyte with 50 µl of 10 mM dimethyl sulfoxide (Alfa Aesar, more than or equal to 99.9%) in D_2O (Sigma-Aldrich, 99.9%) as the internal standard. Deuterated methanol (CD_3OD) concentrations were determined through headspace analysis using a Shimadzu 8050 NX Triple Quadrupole gas chromatograph–mass spectrometry system equipped with a Phenomenex Zebron ZB-WAX column. Calibration curves were obtained using fresh CH_3OH aqueous solutions with different concentrations (0.1, 0.5, 1.0, 1.5 and 2.0 mM) (Supplementary Fig. 9). Quantification of CD_3OD and CH_3OH was performed using characteristic ions of *m/z* 34 and 31, respectively.

Reactivity plot

The presented data with error bars were averages of at least three independent electrolysis experiments. Electrolyte pH was measured before and after each experiment and the measured values are shown in Supplementary Tables 1 and 2. The potential of the Ag/AgCl reference electrode was measured before and after a 30 min electrolysis at −0.72 V versus RHE (the most negative potential investigated) in 0.1 M KOH and no obvious shift in potential was found. In the p_{CO} dependence studies, N_2 and CO were delivered simultaneously at controlled flow rates using mass flow controllers to achieve the desired CO partial pressures. The electrolyte was refreshed after each test and was sampled for NMR analysis. A single CoPc-NH_2/CNT electrode was used throughout a sequence of measurements at different CO partial pressures to eliminate variations between different electrodes.

Data availability

Source data are provided with this paper. All experimental data supporting the findings of this study are available in Supplementary Information.

References

1. Lewis, N. S. Research opportunities to advance solar energy utilization. *Science* **351**, aad1920 (2016).
2. Chu, S., Cui, Y. & Liu, N. The path towards sustainable energy. *Nat. Mater.* **16**, 16–22 (2017).
3. Franco, F., Rettenmaier, C., Jeon, H. S. & Roldan Cuenya, B. Transition metal-based catalysts for the electrochemical CO_2 reduction: from atoms and molecules to nanostructured materials. *Chem. Soc. Rev.* **49**, 6884–6946 (2020).
4. Francke, R., Schille, B. & Roemelt, M. Homogeneously catalyzed electroreduction of carbon dioxide-methods, mechanisms, and catalysts. *Chem. Rev.* **118**, 4631–4701 (2018).
5. Zhang, H., Li, J., Cheng, M.-J. & Lu, Q. CO electroreduction: current development and understanding of Cu-based catalysts. *ACS Catal.* **9**, 49–65 (2018).
6. Nguyen, T. N. et al. Fundamentals of electrochemical CO_2 reduction on single-metal-atom catalysts. *ACS Catal.* **10**, 10068–10095 (2020).
7. Dinh, C. T. et al. CO_2 electroreduction to ethylene via hydroxide-mediated copper catalysis at an abrupt interface. *Science* **360**, 783–787 (2018).
8. Luo, M. et al. Hydroxide promotes carbon dioxide electroreduction to ethanol on copper via tuning of adsorbed hydrogen. *Nat. Commun.* **10**, 5814 (2019).
9. Xia, C. et al. Continuous production of pure liquid fuel solutions via electrocatalytic CO_2 reduction using solid-electrolyte devices. *Nat. Energy* **4**, 776–785 (2019).
10. Monteiro, M. C. O., Philips, M. F., Schouten, K. J. P. & Koper, M. T. M. Efficiency and selectivity of CO_2 reduction to CO on gold gas diffusion electrodes in acidic media. *Nat. Commun.* **12**, 4943 (2021).
11. Weng, Z. et al. Active sites of copper-complex catalytic materials for electrochemical carbon dioxide reduction. *Nat. Commun.* **9**, 415 (2018).
12. Jia, L. et al. Phase-dependent electrocatalytic CO_2 reduction on Pd_3Bi nanocrystals. *Angew. Chem. Int. Ed. Engl.* **60**, 21741–21745 (2021).
13. Guan, A. et al. Boosting CO_2 electroreduction to CH_4 via tuning neighboring single-copper sites. *ACS Energy Lett.* **5**, 1044–1053 (2020).
14. Wang, J., Dou, S. & Wang, X. Structural tuning of heterogeneous molecular catalysts for electrochemical energy conversion. *Sci. Adv.* **7**, eabf3989 (2021).
15. Wu, Y., Liang, Y. & Wang, H. Heterogeneous molecular catalysts of metal phthalocyanines for electrochemical $CO_{(2)}$ reduction reactions. *Acc. Chem. Res.* **54**, 3149–3159 (2021).
16. Cao, R. Across the board: Rui Cao on electrocatalytic CO_2 reduction. *Chem. Sus. Chem.* **15**, e202201788 (2022).
17. Chang, Q. et al. Metal-coordinated phthalocyanines as platform molecules for understanding isolated metal sites in the electrochemical reduction of CO_2. *J. Am. Chem. Soc.* **144**, 16131–16138 (2022).
18. Soucy, T. L. et al. Considering the influence of polymer-catalyst interactions on the chemical microenvironment of electrocatalysts for the CO_2 reduction reaction. *Acc. Chem. Res.* **55**, 252–261 (2022).
19. Zhang, X. et al. Highly selective and active CO_2 reduction electrocatalysts based on cobalt phthalocyanine/carbon nanotube hybrid structures. *Nat. Commun.* **8**, 14675 (2017).
20. Zhang, X. et al. Molecular engineering of dispersed nickel phthalocyanines on carbon nanotubes for selective CO_2 reduction. *Nat. Energy* **5**, 684–692 (2020).
21. Guo, H. et al. Iron porphyrin with appended guanidyl group for significantly improved electrocatalytic carbon dioxide reduction activity and selectivity in aqueous solutions. *Chin. J. Catal.* **43**, 3089–3094 (2022).
22. Ronne, M. H. et al. Ligand-controlled product selectivity in electrochemical carbon dioxide reduction using manganese bipyridine catalysts. *J. Am. Chem. Soc.* **142**, 4265–4275 (2020).
23. Zhang, Z. et al. Reaction mechanisms of well-defined metal-N_4 sites in electrocatalytic CO_2 reduction. *Angew. Chem. Int. Ed. Engl.* **57**, 16339–16342 (2018).
24. Soucy, T. L., Liu, Y., Eisenberg, J. B. & McCrory, C. C. L. Enhancing the electrochemical CO_2 reduction activity of polymer-encapsulated cobalt phthalocyanine films by modulating the loading of catalysts, polymers, and carbon supports. *ACS Appl. Energy Mater.* **5**, 159–169 (2021).
25. Wu, Y. et al. Domino electroreduction of CO_2 to methanol on a molecular catalyst. *Nature* **575**, 639–642 (2019).
26. Boutin, E. et al. On the existence and role of formaldehyde during aqueous electrochemical reduction of carbon monoxide to methanol by cobalt phthalocyanine. *Chem. Eur. J.* **28**, e202200697 (2022).
27. Shi, L. L., Li, M., You, B. & Liao, R. Z. Theoretical study on the electro-reduction of carbon dioxide to methanol catalyzed by cobalt phthalocyanine. *Inorg. Chem.* **61**, 16549–16564 (2022).
28. Boutin, E. et al. Aqueous electrochemical reduction of carbon dioxide and carbon monoxide into methanol with cobalt phthalocyanine. *Angew. Chem. Int. Ed. Engl.* **58**, 16172–16176 (2019).
29. Chen, X., Wei, D. & Ahlquist, M. S. G. Aggregation and significant difference in reactivity therein: blocking the CO_2-to-CH_3OH reaction. *Organometallics* **40**, 3087–3093 (2021).
30. Wu, Y. et al. Heterogeneous nature of electrocatalytic CO/CO_2 reduction by cobalt phthalocyanines. *Chem. Sus. Chem.* **13**, 6296–6299 (2020).

31. Shang, B. et al. Aqueous photoelectrochemical CO_2 reduction to CO and methanol over a silicon photocathode functionalized with a cobalt phthalocyanine molecular catalyst. *Angew. Chem. Int. Ed. Engl.* **62**, e202215213 (2023).
32. Su, J. et al. Improving molecular catalyst activity using strain-inducing carbon nanotube supports. Preprint at *ChemRxiv* https://doi.org/10.26434/chemrxiv-2022-r9r22 (2022).
33. Zeng, J. S., Corbin, N., Williams, K. & Manthiram, K. Kinetic analysis on the role of bicarbonate in carbon dioxide electroreduction at immobilized cobalt phthalocyanine. *ACS Catal.* **10**, 4326–4336 (2020).
34. Li, J. et al. Hydroxide is not a promoter of C_{2+} product formation in the electrochemical reduction of CO on copper. *Angew. Chem. Int. Ed. Engl.* **59**, 4464–4469 (2020).
35. Resasco, J. et al. Promoter effects of alkali metal cations on the electrochemical reduction of carbon dioxide. *J. Am. Chem. Soc.* **139**, 11277–11287 (2017).
36. Zhang, G. et al. Selective CO_2 electroreduction to methanol via enhanced oxygen bonding. *Nat. Commun.* **13**, 7768 (2022).
37. Yang, D. et al. Selective electroreduction of carbon dioxide to methanol on copper selenide nanocatalysts. *Nat. Commun.* **10**, 677 (2019).
38. Guil-Lopez, R. et al. Methanol synthesis from CO_2: a review of the latest developments in heterogeneous catalysis. *Materials* **12**, 3902 (2019).
39. Chang, X. et al. Tuning Cu/Cu_2O interfaces for the reduction of carbon dioxide to methanol in aqueous solutions. *Angew. Chem. Int. Ed. Engl.* **57**, 15415–15419 (2018).
40. Wu, Y. et al. Direct electrosynthesis of methylamine from carbon dioxide and nitrate. *Nat. Sustain.* **4**, 725–730 (2021).
41. Li, J. et al. Electrokinetic and in situ spectroscopic investigations of CO electrochemical reduction on copper. *Nat. Commun.* **12**, 3264 (2021).
42. Ji, Y. L. et al. Selective CO-to-acetate electroreduction via intermediate adsorption tuning on ordered Cu-Pd sites. *Nat. Catal.* **5**, 251–258 (2022).
43. Overa, S. et al. Enhancing acetate selectivity by coupling anodic oxidation to carbon monoxide electroreduction. *Nat. Catal.* **5**, 738–745 (2022).
44. Li, J. et al. Weak CO binding sites induced by Cu-Ag interfaces promote CO electroreduction to multi-carbon liquid products. *Nat. Commun.* **14**, 698 (2023).
45. Yin, Z. et al. An alkaline polymer electrolyte CO_2 electrolyzer operated with pure water. *Energy Environ. Sci.* **12**, 2455–2462 (2019).
46. Fan, L. et al. Electrochemical CO_2 reduction to high-concentration pure formic acid solutions in an all-solid-state reactor. *Nat. Commun.* **11**, 3633 (2020).

Acknowledgements

This work was supported by US National Science Foundation (grant no. CHE-2154724; mechanistic and kinetic studies) and the Yale Center for Natural Carbon Capture (performance and device work).

Author contributions

J.L. and H.W. conceived this project, designed the experiments and wrote the manuscript. J.L. and C.L.R. synthesized the catalyst materials. J.L. performed the electrochemical measurements and analysed the data. B.S., Y.G., S.C. and C.L.R. contributed to data analysis and edited the manuscript. H.W. supervised the project.

Competing interests

The authors declare no competing interests.

Additional information

Supplementary information The online version contains supplementary material available at https://doi.org/10.1038/s44160-023-00384-6.

Correspondence and requests for materials should be addressed to Hailiang Wang.

Peer review information *Nature Synthesis* thanks Zhimin Liu and the other, anonymous, reviewer(s) for their contribution to the peer review of this work. Primary Handling Editor: Alexandra Groves, in collaboration with the *Nature Synthesis* team.